

# The Proton Momentum Distribution in Water and Ice

G.F. Reiter,

*Physics Department, University of Houston, Houston, Texas, USA*

J. C. Li,

*Department of Physics, University of Manchester, PO Box 88, M60 1QD, UK*

J. Mayers, T. Abdul-Redah,

*ISIS Facility, Rutherford -Appleton Laboratory, Chilton, Didcot, OX11 0QX, UK*

and P. Platzman,

*Lucent Technologies, Murray Hill, New Jersey, USA*

Received on 21 October, 2003.

Deep Inelastic Neutron Scattering (Neutron Compton Scattering), is used to measure the momentum distribution of the protons in water from temperatures slightly below freezing to the supercritical phase. The momentum distribution is determined almost entirely by quantum localization effects, and hence is a sensitive probe of the local environment of the proton. The distribution shows dramatic changes as the hydrogen bond network becomes more disordered. Within a single particle interpretation, the proton moves from an essentially harmonic well in ice to a slightly anharmonic well in room temperature water, to a deeply anharmonic potential in the supercritical phase that is best described by a double well potential with a separation of the wells along the bond axis of about 0.3 Angstrom. Confining the supercritical water in the interstices of a C<sub>60</sub> powder enhances this anharmonicity and enhances the localization of the protons. The changes in the distribution are consistent with gas phase formation at the hydrophobic boundaries and inconsistent with the formation of ice there.

## 1 Introduction

The development of pulsed neutron sources such as ISIS at the Rutherford Laboratory in England have, for the first time, made possible the measurement of proton momentum distributions in solids and liquids. These measurements are analogous to the measurement of electron momentum distributions by Compton scattering[1] of light and measurement of nucleon form factors by Deep Inelastic Electron Scattering [2]. The method is known as Neutron Compton Scattering (NCS) or Deep Inelastic Neutron Scattering (DINS). All three techniques rely upon the fact that if the momentum transferred from the incident to target particle is sufficiently large, the impulse approximation (IA) can be used to interpret the data. In the IA, momentum and *kinetic* energy are conserved. From a measurement of the momentum and energy change of the neutron, the momentum of the target nucleus before the collision can be determined. The validity of the impulse approximation is due to the fact that as the momentum transfer increases, the characteristic time for the scattering decreases, and the forces on the particle due to its surroundings have less effect, until in the large q limit, the particle behaves as though it is free for the duration of the scattering event [3]. The scattering at these energies is entirely incoherent, each particle scattering independently.  $S_M(\vec{q}, \omega)$ , the scattering function for a particle of mass M,

is related to the momentum distribution of the particle  $n(\vec{p})$  in this limit by the relation

$$S_M(\vec{q}, \omega) = \int n(\vec{p}) \delta(\omega - \frac{\hbar q^2}{2M} - \frac{\vec{p} \cdot \vec{q}}{M}) d\vec{p} \quad (1)$$

where  $\hbar\omega$  is the energy transfer, M is the mass of the proton, and  $q=|\vec{q}|$  is the magnitude of the wave-vector transfer. The small mass of the proton leads to a broad distribution in energy of the scattered neutrons, centered at  $\frac{\hbar^2 q^2}{2M}$ , that is well separated from the scattering from the heavier ions such as oxygen, which appear as nearly elastic contributions[4]. This, together with its large incoherent cross-section, make hydrogen an ideal candidate for these measurements, although they are feasible on other light ions as well.

## 2 Experimental Setup

The experiments are done on the electron volt spectrometer, Vesuvio, at ISIS. This sort of source is needed to provide high energy neutrons(5-100 eV) for which the energy transfer is sufficiently large compared to the characteristic energies of the system that the scattering is given accurately by the impulse[5] approximation limit. Vesuvio(formerly EVS[6]) is a time-of-flight indirect geometry instrument in which the final state energy of the scattered neutron is fixed

by a resonance filter difference technique[7]. The water and poly-crystalline ice data were taken in standard aluminum sample holders, 10cm by 10cm by 1mm, thin enough to lead to small multiple scattering, which was in all cases, corrected for. A high pressure cell was designed specifically for the high temperature measurements. The background from this ZrTi cell appears as inelastic scattering and is readily subtracted[4]. It can take pressure up to 2000 bar and temperature up to 450°C. The sample size in the cell is 7 mm in diameter and 30 mm in height. The heaters and temperature sensors were all inserted in the cell. A 1 mm steel pipe leads to an external water-pressurizer (i.e. a pump) which provided the required pressure. The water used as pressure transfer media and the sample volume was distilled H<sub>2</sub>O. The smaller volume of water in the beam for the high temperature measurements accounts largely for the poorer statistics. The time scale for the measurements is 10<sup>-15</sup> – 10<sup>-16</sup> sec[3], much shorter than the time for the dissolution of a particular hydrogen bond, so that the momentum distribution we measure can be thought of as resulting from a static local structure.

### 3 Data Analysis

It is clear from Eq. 1 that the measurements do not give directly the momentum distribution, but rather the Radon transform of that distribution. Fortunately, no information is lost from what appears at first sight to be an averaging procedure, and the transform is invertible to obtain  $n(\vec{p})$ . We represent  $S_M(\vec{q}, \omega)$  as  $\frac{M}{q} J(\hat{q}, y)$  where  $y = \frac{M}{q} (\omega - \frac{\hbar q^2}{2M})$ . When the sample is either poly-crystalline or a liquid, the average momentum distribution has no angular dependence, and  $J(\hat{q}, y)$  is independent of  $\hat{q}$ . It is then straightforward to show that  $n(p)$  can be determined from  $J(y)$  as

$$n(p) = \frac{-1}{2\pi y} \left. \frac{\delta J(y)}{\delta y} \right|_{y=p} \quad (2)$$

We will not use this, but fit the data with a series expansion of the form

$$J(y) = \frac{e^{-\frac{y^2}{2\sigma^2}}}{\sqrt{2\pi}\sigma} \sum_n \frac{a_n}{2^{2n} n!} H_{2n} \left( \frac{y}{\sqrt{2}\sigma} \right) \quad (3)$$

where the  $H_n(y)$  are Hermite polynomials.

This series is truncated at some order ( $2n = 14$  in this case). The coefficients  $a_n$  then determine the measured  $n(p)$  directly as a series in Laguerre polynomials [4]:

$$n(p) = \frac{e^{-\frac{p^2}{2\sigma^2}}}{(\sqrt{2\pi}\sigma)^3} \sum_n a_n (-1)^n L_n^{\frac{1}{2}} \left( \frac{p^2}{2\sigma^2} \right) \quad (4)$$

A relation between the derivative of Hermite polynomials and Laguerre polynomials[8] ensures that Eq. 2 is satisfied.

The procedure is a smoothing operation, which works with noisy data, and which also allows for the inclusion

of small corrections to the impulse approximation[4, 9]. The leading term of the correction has the functional form  $H_3(y)/q$ . This is added to the expansion in Eq. 3 with an undetermined coefficient. The entire expression is then convolved with the instrumental resolution function and fit to the data to determine the coefficients in the expansion. The errors in the measured  $n(\vec{p})$  are determined by the uncertainty in the the measured coefficients, through their correlation matrix, which is calculated by the fitting program. The uncertainty in the measurement of  $n(\vec{p})$  at some point  $\vec{p}$  is due to the uncertainty in the measured coefficients. Denoting an arbitrary coefficient by  $\rho_i$ , we have

$$\delta n(\vec{p}) = \sum_i \frac{\delta n(\vec{p})}{\delta \rho_i} \delta \rho_i \quad (5)$$

The fitting program, after a minimum is obtained with some set of coefficients, calculates the correlation matrix  $\langle \delta \rho_i \delta \rho_j \rangle$  [10]. Hence, the variance in the momentum distribution is

$$\langle \delta n(\vec{p})^2 \rangle = \sum_{i,j} \frac{\delta n(\vec{p})}{\delta \rho_i} \frac{\delta n(\vec{p})}{\delta \rho_j} \langle \delta \rho_i \delta \rho_j \rangle \quad (6)$$

A further refinement is that we set the coefficient  $a_1$  to zero in the expansion. This is necessary because the scale factor,  $\sigma$ , in Eq. 3 is undetermined. The expansion is true for any value of  $\sigma$ . As a consequence, the coefficient  $a_1$  and the Gaussian scale factor  $\sigma$  in the expansion are strongly correlated in the least squares fit, leading to indeterminacy in the fits if both  $a_1$  and  $\sigma$  are varied. Setting  $a_1$  to zero has the further benefit that the total kinetic energy is then determined entirely by  $\sigma$ , even for strongly anharmonic momentum distributions [11]. In units in which  $\sigma$  is measured in Å<sup>-1</sup>, and the energy is expressed in milli-electron volts, the total kinetic energy (for a proton) is K.E.=6.2705σ<sup>2</sup>.

### 4 Experimental Results

When fit in the way described above, which we will call a free fit,[10] since there is no model assumed, we find that in fact there are at most two coefficients that are statistically significant,  $a_2$  and  $a_3$ , for all the data except the room temperature water, where  $a_5$  and  $a_6$  are significant (barely). We will consider room temperature water in more detail below. In order to make clear that the changes we see are not due to differences in the fitting functions used, we will present the results for all the fits with only  $a_2$  and  $a_3$  included in the expansion. It is these coefficients, together with  $\sigma$ , that we present in the Table 1 to describe  $n(p)$ .

Table 1. Parameters for Free Fit

Water Sample	$\sigma(\text{\AA}^{-1})$	$a_4$	$a_6$
Ice -4C	4.579	$0.060 \pm 0.0014$	$-0.068 \pm 0.016$
Water 23C	4.841	$0.185 \pm 0.012$	$0.015 \pm 0.015$
T=400C, P=750bar	6.363	$0.271 \pm .022$	$0.157 \pm 0.028$
T=400C, P=750bar in C <sub>60</sub>	6.439	$0.592 \pm 0.054$	$0.007 \pm 0.07$

The values of  $\sigma$  are not given error bars because in the final fit, they are taken as scale parameters.

## 5 Interpretation of the Data

This representation should be regarded as the data for  $n(p)$  determined by the measurement. We show in Fig. 1 a comparison of the free fits to the data for ice, water at room temperature, supercritical water, and supercritical water contained in the interstices of a C<sub>60</sub> powder. The typical size for the interstices is 100Å. The quantity  $4\pi p^2 n(p)$ , the radial momentum distribution is presented, in order to compare quantities with the same normalization.

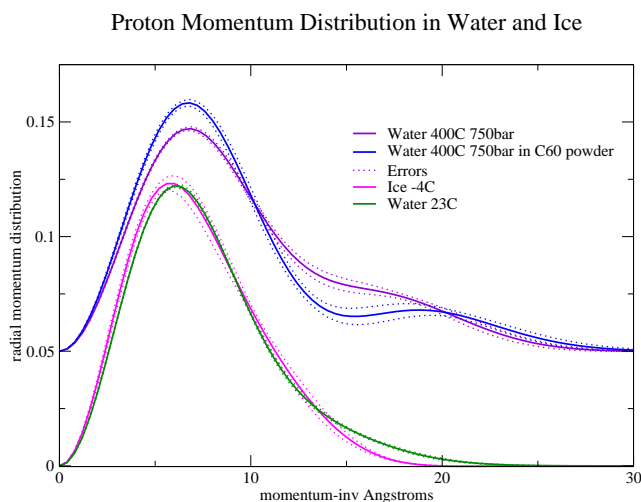


Figure 1. Comparison of fits to the data of the radial momentum distribution,  $4\pi p^2 n(p)$  for a range of conditions from ice to supercritical water, to supercritical water in the interstices of a C<sub>60</sub> poly-crystalline powder, corresponding to increasing disorder in the hydrogen bond network. The 400°C data has been shifted up for clarity.

The kinetic energy due to the temperature has a small effect on the momentum distribution. Even at the highest temperature, the thermal kinetic energy corresponds to a momentum width of only about  $3 \text{\AA}^{-1}$ . The corrections to the momentum widths for the ice due to the finite temperature, are negligible along the bond and only a few percent transverse to the bond. What we are seeing is nearly entirely a quantum effect, reflecting the local structure of the proton environment. The structural changes in going from ice to water are noticeable in the data. The tail of the distribution is due to the momentum along the bond direction, since the proton is most tightly bound in this direction, and it is clear

that this width has increased. The shift to a higher momentum width along the bond axis can be interpreted as due to the slight increase in the average hydrogen bond distance, so that the proton becomes more tightly bound to its covalently bonded oxygen. The change in the covalent bond length is only about 4% but the measurements are clearly accurate enough to see this shift. This interpretation can also be applied to the supercritical water data, where the density is only 0.65 gr/cc, explaining the greatly increased momentum width. However, the second peak in that data, is entirely unexpected from this simple picture of the bond. One could try to interpret the second peak as a small population of protons with unusually high momentum. However, this would mean an rms energy of these protons of approximately 2.5 eV, and a localization length of about 0.05 Angstrom. We know of no mechanism for producing such energetic protons, and will not consider this possibility further. We will interpret the data in terms of a single particle in an effective potential due to its neighbors. With this interpretation, the second peak indicates that the proton is coherent over two separated sites along the bond. This can be made clear by fitting the data phenomenologically.

To a first approximation, since the proton is surrounded by much heavier oxygen atoms, the proton momentum distribution can be thought of as arising from its confinement in the potential well provided by the oxygens[12], which can be regarded as fixed in position. The interaction with other protons will modify this potential well. While their effect cannot be truly regarded as arising from a static potential, we will assume, in the spirit of a mean field approximation, that they provide an effective potential for the protons. We can then calculate the momentum distribution as though we had a single particle in a fixed effective potential. In fact, we will define the effective potential as the one that produces the observed momentum distribution when interpreted this way.

We will assume a model, in which, in a frame of reference in which an individual bond is taken to lie along the z axis, the motion transverse to the bond is harmonic and along the bond given by a wavefunction that corresponds in real space to two Gaussians separated by a distance  $d$ . We will also assume  $\sigma_x = \sigma_y$ . We have done fits with this condition relaxed, and find that it is well satisfied. The parameter  $\sigma_z$  gives the width of the Gaussians in real space through the uncertainty relation. In the case that  $d=0$ , we have an

anisotropic Gaussian momentum distribution.

$$n(p_x, p_y, p_z) = \frac{2\cos^2(\frac{p_z d}{2\hbar})}{1 + e^{-\frac{d^2 \sigma_z^2}{2\hbar^2}}} \prod_i \frac{e^{-\frac{p_i^2}{2\sigma_i^2}}}{(2\pi\sigma_i)^{\frac{1}{2}}} \quad (7)$$

This Gaussian distribution is then averaged over all angles, the corresponding  $J(y)$  fit to the data, and the parameters of the model determined. It is the case that an anisotropic Gaussian, when spherically averaged, is not Gaussian, but has an expansion in the form of Eq. 3, in which  $\sigma^2 = (2\sigma_x^2 + \sigma_z^2)/3$  and the anharmonic terms are determined by the difference between the momentum widths parallel and perpendicular to the bond[13].

We show in Fig. 2 the fits to that model, and in Table 1 the parameters obtained for those fits. The ice data is very accurately described by an anisotropic Gaussian. The parameters of the Gaussian correspond to vibrational energies in the transverse and longitudinal directions of 105 meV and 332 meV respectively. The water data is also well described this way, with a higher stretch frequency of 367 meV and no change in the transverse frequency, although there are clearly additional anharmonicities that make small correc-

tions that are visible in the figure. These may be due to a variation of the effective potential from site to site in the water. Indeed, if the distribution were due entirely to a rotationally averaged gaussian, the coefficient of  $a_3$  would have to be negative, and it is not[13]. It may be due as well, however, to an intrinsic anharmonicity in a single bond, perhaps the precursor to the strong anharmonicity seen in the supercritical water data. Li et al[14] have measured the frequency of vibration for hydrogen impurities in  $D_2O$  ice, which should be comparable to the frequencies we infer from the anisotropic harmonic fit to our data. They find that the two transverse vibrations are at 105 meV and 200 meV, with the stretch mode at 405 meV. The additional contributions to the anharmonic coefficients may be responsible for the discrepancy with Li et al's results, since the difference in the transverse mode frequencies we obtain by fitting is very sensitive to the value of  $a_3$ .

The fits to the supercritical data require non zero values for the parameter  $d$  giving the separation of minima in the potential wells. That is the proton is coherent over sites separated by a distance of approximately 0.3 Angstrom that are both local minima of the potential.

Table 2. Parameters for Model Fit

Water Sample	$\sigma_z(\text{\AA}^{-1})$	$\sigma_x(\text{\AA}^{-1})$	$d(\text{\AA})$
Ice -4C	$6.29 \pm 0.51$	$3.53 \pm 0.31$	0
Water 23C	$6.73 \pm 0.08$	$3.51 \pm 0.04$	0
T=400C, P=750bar	$8.40 \pm 0.19$	$5.70 \pm 0.16$	$0.316 \pm 0.0045$
T=400C, P=750bar in $C_{60}$	$9.47 \pm 0.26$	$5.025 \pm 0.11$	$0.274 \pm 0.0043$

### Comparison With One-Particle Model

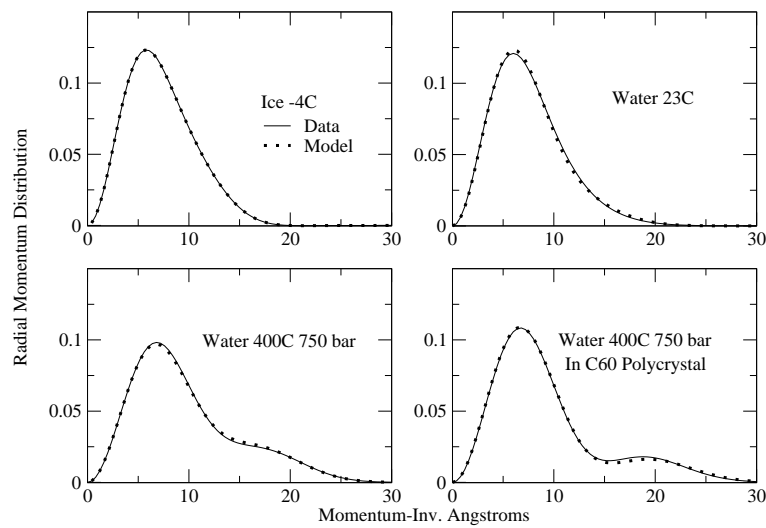


Figure 2. Comparison of radial momentum distribution,  $4\pi p^2 n(p)$  with an effective one-particle model based on double wells along the bond direction. (Eq.7). The additional peaks in the supercritical water data are attributed to coherence over wells separated by distances of the order of 0.3 Angstrom in this model. There is only one well for the room temperature water and the ice data.

We know of no prediction of such an effect. The disorder in the hydrogen bond network would lead to bifurcated bonds, double bonds, bent bonds and missing bonds. It would seem that these would lead to tunnelling motions transverse to the bond. In our experiment, however, the tunnelling, or more precisely, the coherence, shows up along the axis with a high momentum width, which is surely the axis of stretching of the covalent bond. To the extent that there are linear bonds, this would be the bond axis. In fact, it is reasonable to think that the supercritical water is made up of small clusters that combine and break up on a time scale much longer than our observation time, so we are seeing a snapshot average of the ground states for the proton in these small clusters. It is possible then, that what we are seeing is the effect of cooperative tunnelling between bifurcated bonds and single bonds, as observed in trimers and small clusters [15]. Although the cooperative tunneling motion in these small clusters involves primarily the transverse motion, this could be accompanied by changes in the length of the covalent bond, which is what we see. It is also the case that the temperature is higher than the tunnel splitting in small clusters[15] so we would not expect to see the transverse coherence even if the interference it produces occurred at a sufficiently small momentum as to be observable.

The wells are sufficiently separated that the wavefunction actually becomes bimodal. We show in Fig. 3 the probability, (the wave-function squared) corresponding to the fitted momentum distributions for the four measurements, together with the potential that would produce that wavefunction.

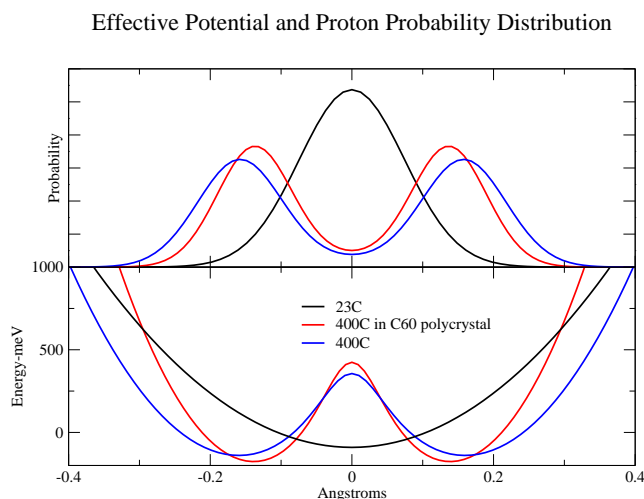


Figure 3. Comparison of probability, based on an effective single particle model, for finding proton at a position along the bond. The zero position is unknown from our experiments, so that the coordinate is relative to the most probable position. The ice and room temperature results are Gaussian, corresponding to harmonic wells. The high temperature wavefunctions are assumed to be the sum of two Gaussians separated by some distance (Table 2), and the potential is that which would produce those wavefunctions.

We note that the interpretation in terms of a single par-

ticle effective potential, although it describes the data well, is not entirely consistent. The tunnel splitting in the two high temperature effective potentials is about 35 meV. With the temperature approximately 70 meV, the two lowest levels would be nearly equally populated, and the coherence in the ground state would not be observable. The effective potential is then only a phenomenological representation of a more complex many-body phenomenon.

For the water in the interstices of the powdered  $C_{60}$ , one can expect that the the hydrogen bond network will be even more distorted than in the pure water, and we will be seeing an average over bonds that are near the surface with those that are relatively “in the bulk”. The size of the surface layer at ordinary temperatures is in some dispute[16, 17], ranging from 1.5-5nm and it seems certain that it would be significantly larger for the supercritical water. It is conceivable, given the size of the interstices in the  $C_{60}$  poly-crystal, that the entire volume of water would be strongly affected by the contact with the surfaces. Consistent with this, we find that the protons are more localized in the  $C_{60}$  interstices than in the “free” supercritical water, with both the width of the individual Gaussians in the spatial wave function and their separation decreasing when the water is contained in the  $C_{60}$  interstices.

There is no sign of ice formation at the surfaces. This might be regarded as not terribly surprising, given the temperature, but the bond energies involved are still large compared to the temperature, and it is conceivable that the presence of the repulsive surface would be sufficient to cause the ice phase to form. We would expect then to see a narrowing, rather than a broadening, of the distribution. In any case, the results are consistent with the formation of the gas phase there. Indeed the kinetic energy for the supercritical water ( $25 \pm 6$  meV is slightly greater than that calculated for the free water molecule (214 meV) at the same temperature and pressure [18].

As is clear from Fig. 2, the room temperature water data is not fit perfectly by the anisotropic Gaussian model. We show in Table 3 a more refined fit of the data with coefficients up to  $a_6$  included, compared with the prediction from the anisotropic Gaussian model. The deviations from this model may have many sources. Additional averaging, over and above the rotational averaging that has been used to generate the coefficients in the table, due to fluctuations in the curvature of the potential from site to site, or intrinsic anharmonic terms in the potential, or many body effects not included in our analysis, could lead to these deviations. There is no way to separate these effects experimentally. The data in Table 3 may prove useful, however, for comparing simulations of the momentum distribution based on model potentials or ab-initio methods, should these become available. In this regard, we point out that while classical simulations of room temperature water or ice may be adequate for calculating structure(spatial correlations) they are unlikely to

give accurate results for supercritical water. At low temperatures, when the potential is harmonic, the centroid of the proton wavefunction is all that is needed to describe the motion. That can be done classically, as there is no distortion of the shape of the Gaussian wave packet as the proton moves. However, the strong anharmonicity present in the effective potential at high temperatures, whatever its origin, would couple the centroid motion with changes in the shape of the wave function, an effect that can not be included in a classical calculation.

Table 3. Comparison of an extended fit of the data for room temperature water with those derived from a rotationally averaged anisotropic Gaussian model.

Coefficient	Water Data 23°C	Model Prediction
$\sigma$	$4.848 \text{ \AA}^{-1}$	$4.827 \text{ \AA}^{-1}$
$a_2$	$0.205 \pm 0.020$	0.168
$a_3$	$0.053 \pm 0.045$	-0.044
$a_4$	0	-0.061
$a_5$	$-0.099 \pm 0.093$	-0.034
$a_6$	$-0.094 \pm 0.078$	-0.032

## 6 Conclusions

In conclusion, the results shown here, in addition to providing a detailed picture of the dynamics of the proton in water, show that the momentum distribution of the proton, which is sensitive to the local structure of the proton, can be measured with sufficient accuracy to provide detailed information about that structure, even in liquids or powder samples.

### Acknowledgements

One of us (G.R.) would like to thank Tony Haymet and Ariel Chialvo for useful discussions.

## References

- [1] P. M. Platzmann in *Momentum Distributions*, ed R. N. Silver and P. E. Sokol (Plenum Press, New York, 1989, p249).

- [2] I. Sick in ref 1, page 175.
- [3] R. Silver and G. Reiter, *Phys. Rev. Letts.* **54**, 1047 (1985).
- [4] G. Reiter, J. Mayers, and J. Noreland, *Phys. Rev. B* **65**, 104305 (2002).
- [5] P. M. Platzmann, in *Momentum Distributions*, ed R. N. Silver and P. E. Sokol (Plenum Press, New York, 1989, p249).
- [6] J. Mayers and A. C. Evans, Rutherford Appleton Laboratory Report No. RAL-TR-96-044, 1996(unpublished).
- [7] P. A. Seeger, A. D. Taylor, and R. M. Brugger *Nuc. Inst. Meth.* **A240**, 98 (1985).
- [8] M. Abramowitz and I. Stegun, *NBS Applied Mathematics Series* **55**, P779, (1964).
- [9] V. F. Sears, *Phys. Rev.* **185**, 200 (1969); *Phys. Rev. A7*, 340 (1973).
- [10] D. Sivia, *Data Analysis: A Bayesian Tutorial*, Clarendon Press, Oxford (1996).
- [11] By definition the kinetic energy is  $\int \frac{p^2}{2M} n(\vec{p}) d\vec{p}$ . Representing  $p^2$  as  $-L_1^{\frac{1}{2}} + \frac{3}{2}$ , using Eq. 4 for  $n(p)$ , and observing that the Laguerre polynomials are orthogonal with the weighting in that equation, we obtain K.E. =  $\frac{3}{2M} \sigma^2$  when  $L_1^{\frac{1}{2}}$  is omitted from the sum in Eq. 4.
- [12] M. Warner, S. W. Lovesey, and J. Smith, *Z. Phys. B* **39**, 2022 (1989).
- [13] The average may be done analytically. For the case that the two transverse directions have the same variance, we find  $\langle J(y) \rangle$  is of the form given in Eq.3, with  $a_1 = 0$ ,  $\sigma^2 = (2\sigma_x^2 + \sigma_z^2)/3$ , and  $a_n = (\frac{\delta\sigma^2}{\sigma^2})^n < (1/3 - \cos^2(\theta))^n >$ , where  $\delta\sigma^2 = (\sigma_x^2 - \sigma_z^2)$ . Explicitly,  $a_2 = 4/45 (\frac{\delta\sigma^2}{\sigma^2})^2$  and  $a_3 = 16/945 (\frac{\delta\sigma^2}{\sigma^2})^3$ .
- [14] J. C. Li, *J. Chem. Phys.* **105**, 6733, (2003).
- [15] F. N. Keutsch and R. J. Saykally, *Proc. Nat. Acad. Sci.* **98**, 10533 (2001).
- [16] T. R. Jensen *et al.*, *Phys. Rev. Lett.* **90**, 86101 (2003).
- [17] R. Steitz *et al.*, *Langmuir*, **19**, 2409 (2003).
- [18] C. H. Uffindell, A. I. Kolesnikov, J. C. Li, and J. Mayers, *Phys. Rev. B* **62**, 5492 (2000).